

RESEARCH ARTICLE

10.1002/2015MS000474

Effects of vertical wind shear on the predictability of tropical cyclones: Practical versus intrinsic limit

Dandan Tao¹ and Fuqing Zhang¹

¹Department of Meteorology, Pennsylvania State University, University Park, Pennsylvania, USA

Key Points:

- Predictability of TCs varies under different environmental shear conditions
- The larger the shear, the less predictable the TCs until the shear is too large
- There are limits in both practical and intrinsic TC predictability

Correspondence to:

F. Zhang,
fzhang@psu.edu

Citation:

Tao, D., and F. Zhang (2015), Effects of vertical wind shear on the predictability of tropical cyclones: Practical versus intrinsic limit, *J. Adv. Model. Earth Syst.*, 07, doi:10.1002/2015MS000474.

Received 22 APR 2015

Accepted 7 SEP 2015

Accepted article online 11 SEP 2015

Abstract The effects of environmental shear on the dynamics and predictability of tropical cyclones (TCs) are further explored through a series of cloud-permitting ensemble sensitivity experiments with small, random initial condition perturbations on the low-level moisture fields. As an expansion of earlier studies, it is found that larger the shear magnitude, less predictable the TCs, especially the onset time of the rapid intensification (RI), until the shear is too large for the TC formation. Systematic differences amongst the ensemble members begin to arise right after the initial burst of moist convection associated with the incipient vortex. This randomness inherent in moist convection first changes the TC vortex structure subtly, but the location and strength of subsequent moist convection are greatly influential to the precession and alignment of the TC vortex as well as the RI onset time. Additional ensemble sensitivity experiments with different magnitude random perturbations to the mean environmental shear (6 m s^{-1}) show that when the standard deviation of the random shear perturbations among different ensemble members is as small as 0.5 m s^{-1} , the difference in shear magnitude overwhelms the randomness of moist convection in influencing the TC development and rapid intensification (indicative of limited practical predictability). However, for the ensemble with standard deviation of 0.1 m s^{-1} in random shear perturbations, the uncertainty in TC onset timing is comparable to the ensemble that is perturbed only by small random moisture conditions in the initial moisture field (indicative of the limit in intrinsic predictability).

1. Introduction

Environmental shear has long been recognized to be influential to TC formation and intensification [DeMaria, 1996; Frank and Ritchie, 2001; Moskaitis, 2010] while a large number of TC genesis events happen under vertical wind shear [Nolan and McGauley, 2012]. Furthermore, it is known that errors in the prediction of vertical wind shear in the vicinity of a TC will lead to large errors in the forecast of the storm's intensity [Emanuel et al., 2004; DeMaria and Kaplan, 1999; Munsell et al., 2013]. A better understanding of the effects of vertical wind shear on TCs, including its role in the predictability of storm development, is necessary to improve forecast accuracy.

A TC vortex embedded in vertical wind shear is first tilted and promotes the formation of an asymmetric secondary circulation with upward motion in the same direction as the tilt (i.e., "down-tilt") and downward motion in the "up-tilt" (opposite) direction [Jones, 1995; Wong and Chan, 2004]. Many studies have observed that vertical wind shear will induce great asymmetry in the spatial distribution of TC rainfall [Rogers et al., 2003; Chen et al., 2006]. Besides this shear-induced asymmetry, the TC vortex under vertical wind shear will undergo two processes of precession and alignment as well [Jones, 1995; Reasor and Montgomery, 2001; Davis et al., 2008; Davis and Ahijevych, 2012; Rappin and Nolan, 2012]. However, the cause of precession and alignment is still under investigation. Some studies [Jones, 2004; Reasor et al., 2004] showed that the vortex could precess and align under dry dynamics. At the same time, there are other studies [Frank and Ritchie, 1999; Davis et al., 2008] emphasizing the role of diabatic heating on precession and alignment. For example, Frank and Ritchie [1999] found that the vortex in moist simulation could survive the vertical wind shear and intensify while dry vortex fails to precess and align. Moreover, Davis et al. [2008] note that diabatic heating in the down-tilt direction acts to reduce tilt magnitude. Taken together, all of these results indicate that the effect of moist convection on the precession and alignment of a sheared TC vortex cannot be underestimated.

At the same time, a source of significant uncertainty is found to be from random, chaotic moist convection, which may ultimately limit the predictability of TCs; even minute, virtually unnoticeable differences in the

© 2015. The Authors.

This is an open access article under the terms of the Creative Commons Attribution-NonCommercial-NoDerivs License, which permits use and distribution in any medium, provided the original work is properly cited, the use is non-commercial and no modifications or adaptations are made.

initial conditions can dramatically alter the development of a TC [e.g., Sippel and Zhang, 2008, 2010; Nguyen et al., 2008; Zhang and Sippel, 2009; Zhang and Tao, 2013; Taraphdar et al., 2014]. For example, Nguyen et al. [2008] found that small, random moisture perturbations in the boundary layer can greatly change the flow asymmetry due to bursts of deep convective vortex structures. Sippel and Zhang [2008] studied a nondeveloping tropical disturbance by utilizing short-range ensemble forecasts to elucidate why some ensemble members strengthened the disturbance into a TC but other members did not. They found that differences in deep moisture and convective available potential energy caused much of the initial ensemble spread and these discrepancies were subsequently further amplified by differences in convection-related latent heat fluxes and the wind-induced surface heat exchange (WISHE) process [Emanuel, 1986; Rotunno and Emanuel, 1987]. Zhang and Sippel [2009] traced the differences between two divergent members of the Sippel and Zhang [2008] ensemble to the effects of moist convection, and showed that the intrinsic predictability of TCs can be limited by small-scale variations in the initial conditions, which may cause dramatic differences during TC formation. Taraphdar et al. [2014] further found that the error growth of Indian Ocean TCs is similar to that of midlatitude extratropical cyclones [Zhang et al., 2002, 2003, 2007], which first comes from moist convection before ultimately affecting storm-scale circulations.

The combined effects of moist convection and vertical wind shear on the predictability of TC intensity were examined through idealized simulations [Zhang and Tao, 2013, hereafter ZT13]. It was found that small-amplitude initial perturbations in the low-level mixing ratio can lead to variations in the RI onset time (The Rapid Intensification (RI) onset time is defined as the start time of continuous rapid intensification for 24 h. RI here is defined as the increase in the maximum 10 m winds of a tropical cyclone more than 15.4 m s^{-1} in a 24 h period.) of as much as 2 days (given environmental vertical wind shear of 5 m s^{-1}). The systematic difference between members in one ensemble set is first seen in the vortex tilt and subsequently the timing of precession and alignment processes. In that paper, we hypothesized that this systematic deviation between members are coming from the small, random differences in moist convection among ensemble members, which indicates the intrinsically limited predictability of TC intensity under moderate vertical wind shear. Tao and Zhang [2014, hereafter TZ14] further explored from an ensemble-mean perspective the impacts of different shear magnitudes on the distribution and organization of the convection and the diabatic-heat-driven secondary circulation. It was found that larger shear magnitudes forcing the convection farther away from the center make the insufficient convergence of angular momentum, yielding a weaker vortex and making it more difficult for the convection to become axisymmetric.

Complementary to ZT13 and TZ14, the current study further explores the predictability of TC genesis and RI under a wider range of vertical wind shear scenarios as well as the role of moist convection on forming the differences between the members. Moreover, this work systematically addresses both the practical and intrinsic aspects of TC predictability with regards to the sensitivity of TC formation and RI to minute, random initial moisture perturbations and to different magnitude of environmental shear uncertainty. Here practical predictability is defined as the limit of predictability given the current accuracy of forecast models and initial conditions whereas intrinsic predictability refers to the predictability under nearly perfect model and almost unnoticeable initial errors [Lorenz, 1996; Melhauser and Zhang, 2012].

This paper is organized as follows. Section 2 presents the experimental design. The overall intensity evolutions of ensemble sets are described in section 3. A detailed analysis of selected members is presented in section 4. Correlation and error growth analyses are performed in section 5. The “fake-dry” sensitivity experiments that turn off the diabatic heating associated with water phase changes are explored in section 6. Comparison of intrinsic versus practical predictability is presented in section 7. Finally, our conclusions are discussed in section 8.

2. Experimental Design

As in ZT13, Version 3.1.1 of the Weather Research and Forecasting (WRF) model is used for all the simulations in this study. The initial vortex is an idealized modified Rankine vortex with maximum surface wind speed of 15 m s^{-1} at a 135 km radius. The domain is set on a doubly periodic f-plane with a constant Coriolis parameter equivalent to 20°N . The moist tropical sounding of Dunion [2011] is used to set up the thermodynamic environment, and all experiments have a constant sea-surface temperature of 27°C . The varying factor between sets is the background flow (vertical wind shear magnitude). The vertical profiles of the

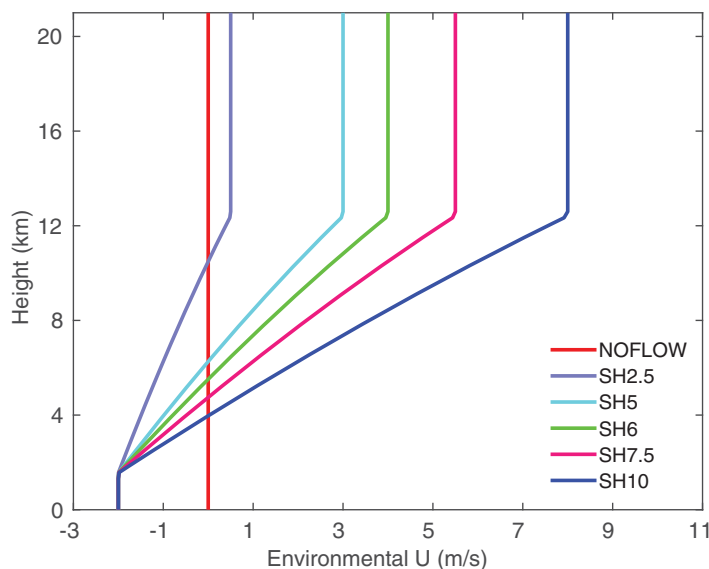


Figure 1. Vertical profiles of environmental flow for NOFLOW, SH2.5, SH5, SH6, SH7.5, and SH10.

environmental flows for all ensemble experiments are shown in Figure 1. There is no environmental mean flow or vertical wind shear in ensemble experiments “NOFLOW.” The other experiments (namely “SH2.5,” “SH5,” “SH6,” “SH7.5,” “SH10”) have westerly vertical wind shear of 2.5, 5, 6, 7.5, and 10 m s^{-1} , respectively, between 200 and 850 hPa; below the 850 hPa level, all shear experiments have the same low-level easterly wind of 2 m s^{-1} . The “point-downscaling” method [Nolan, 2011] is used to force the vertical wind shear (with no temperature gradient) throughout the simulation time.

As in ZT13 and TZ14, the ensemble members are created by applying 20 realizations of moisture perturbations with magnitudes randomly selected from a uniform distribution of $(-0.5, 0.5) \text{ g kg}^{-1}$ to the initial mixing ratio fields throughout the innermost domain below 950 hPa. In section 5, we added five sets of same kind of moisture perturbation to SH5 control run (the simulation with unperturbed initial condition) at simulation time of 24, 48, and 72 h (denoted by adding a suffix of “dayN,” N is the number of control simulation days). Furthermore, the “fake-dry” sensitivity experiments (denoted by FD48 and FD48-72) are carried out in section 6 by turning off the latent heating associated with water phase changes (“cu_physics = 0” and “no_mp_heating = 1” in the WRF namelist).

As in ZT13 and TZ14, the ensemble

Two additional sets of ensembles are generated to investigate the sensitivity to small differences in vertical wind shear (section 7). In one ensemble set (“SH6-STD0.1”), each member is assigned a slightly different value of shear magnitude by drawing from a normal distribution centered on 6 m s^{-1} with a standard deviation of 0.1 m s^{-1} ; in the other ensemble set (“SH6-STD0.5”), the shear magnitudes are determined the same way except using a larger standard deviation of 0.5 m s^{-1} . The shear values for each member of these two perturbed shear sensitivity experiments are listed in Table 1.

3. Forecast Uncertainty Versus Vertical Wind Shear

First, we examine the temporal evolution of TC intensity (in terms of maximum 10 m wind speed) for the experiments with different shear (Figure 2). The NOFLOW and SH5 cases (Figures 2a and 2c) are the same as discussed in ZT13 (their Figures 2a and 2d). It is quite clear that the larger the shear, the larger the spread in RI onset time between members (Figures 2b–2e), which is consistent with ZT13 (their Figures 2b–2d). It is also evident that there is a maximum shear threshold for TC development under given environmental and initial TC conditions. A shear magnitude of 7.5 m s^{-1} or larger (we performed, but do not show, experiments with shear of 10 m s^{-1}) prevents any TC development/RI during the 9 day simulation window. In addition, the ensemble mean and spread of RI onset do not increase linearly with shear magnitude: an increase in shear of only 1 m s^{-1} from 5 to 6 m s^{-1} shifts the entire range of RI onset times to 2 days later and enlarges the spread from ~ 2 to ~ 3 days. It is interesting to combine the SH5, SH6, and SH7.5 experiments into one large ensemble (Figure 2f). The RI onset time in this combined ensemble varies widely, ranging from 96 h (for smaller shear) to no RI during the entire 216 h simulation period (for larger shear). This extremely large uncertainty in RI onset given modest uncertainty in environmental shear and minute initial moisture perturbations may contribute to the challenges associated with the practical predictability of TCs (as discussed further in section 7). This also indicates

Table 1. List of Shear Conditions and Approximate RI Onset Times for Each Member in SH6-STD0.1 and SH6-STD0.5

Member	SH6-STD0.1		SH6-STD0.5	
	Shear (ms ⁻¹)	Onset Time (h)	Shear (ms ⁻¹)	Onset Time (h)
EN10	6.0096	157	6.0692	151
EN11	5.917	156	5.0465	124
EN12	5.9648	183	5.8175	162
EN13	5.9825	186	5.5759	159
EN14	5.9519	168	5.6176	150
EN15	6.0837	162	5.4362	147
EN16	6.2538	172	6.0391	129
EN17	5.8677	141	7.0533	N/A
EN18	6.0128	182	5.6421	159
EN19	5.8558	163	5.8597	132
EN20	6.1303	178	6.5832	198
EN21	6.141	182	6.6064	N/A
EN22	5.8337	145	6.2428	175
EN23	6.1944	161	6.513	N/A
EN24	5.8915	184	6.4354	N/A
EN25	6.0227	196	5.8091	204
EN26	6.1099	152	6.2144	197
EN27	6.0147	156	5.8504	149
EN28	6.2296	173	5.5501	144
EN29	6.2753	N/A	6.3174	170

that when there is error in the shear, forecasts of TC development can be extremely inaccurate, which is also consistent with the findings of Emanuel et al. [2004].

One thing we need to mention is that all the results above are from the specific vortex and environmental setups. Actually when the initial vortex is weaker (maximum surface wind is 10 m s⁻¹), the storm cannot develop even under 5 m s⁻¹ shear (not shown).

In order to highlight the differences that these small initial moisture perturbations can induce, we choose three exemplar members from SH5 (SH5-Early, SH5-Medium, and SH5-Late, Figure 2c); these same three members were highlighted in ZT13. For further comparison, we also pick

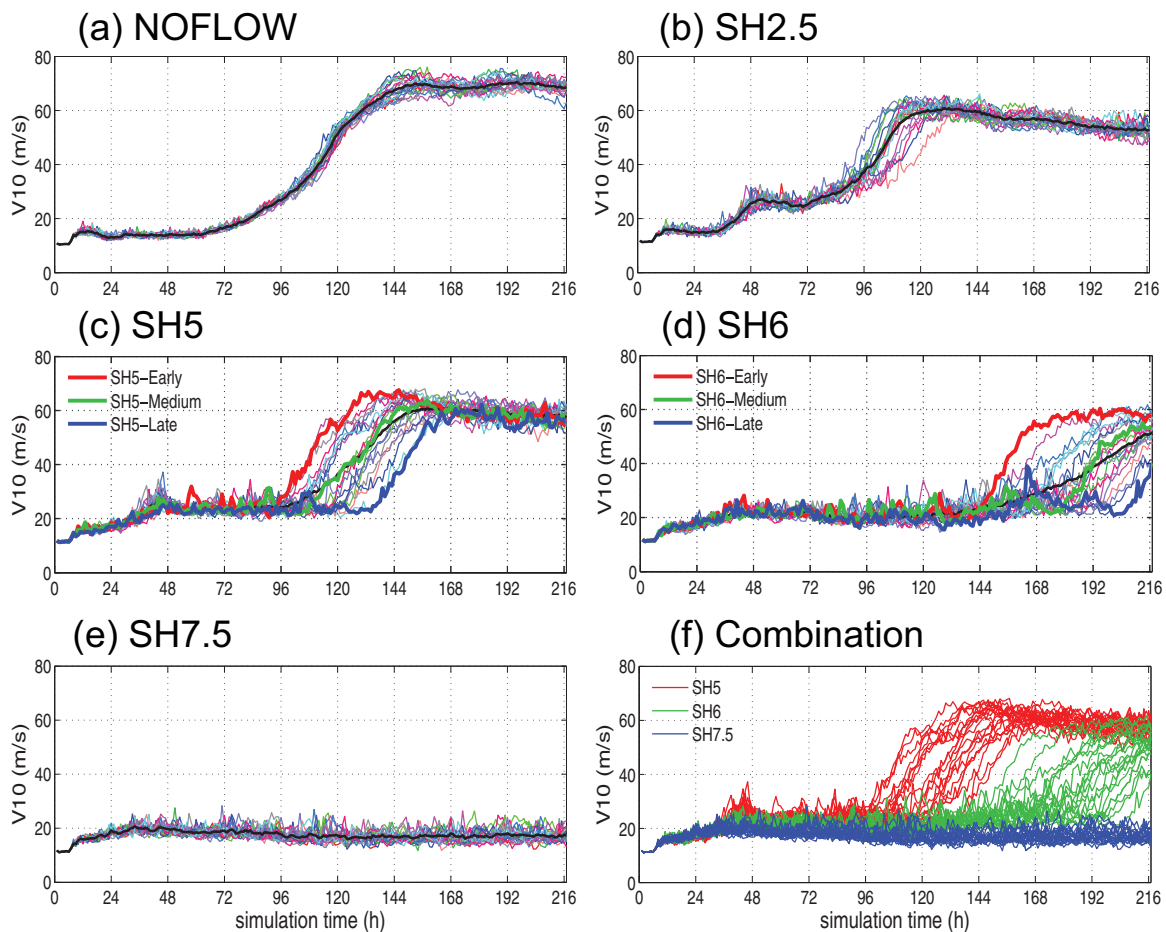


Figure 2. Time evolution of the tropical cyclone intensity in terms of the 10 m maximum wind speed for all ensemble members of (a) NOFLOW, (b) SH2.5, (c) SH5, (d) SH6, (e) SH7.5, and (f) combination of SH5, SH6, and SH7.5. All under SST = 27°C.

three typical members from SH6 (which has the largest ensemble spread in Figure 2), with SH6-Early having the earliest RI onset time, SH6-Medium an average RI onset time, and SH6-Late the latest RI onset time (Figure 2d). Detailed analyses of these selected members are presented below.

4. Shear, Tilt, and Diabatic Heating Evolution for the Selected Members

Though the members within the same ensemble have no apparent differences in the evolution of the maximum 10 m winds prior to RI onset, there are considerable variations in the evolution of the vortex structures (tilt vector as a representative) of these members during this early period. The tilt vector is calculated as the difference between the positions of the vorticity-weighted centers at 850 and 450-hPa, and the local vertical shear vector is defined as the difference between the horizontal winds at the 850 and 450 hPa levels averaged within 300 km radius of the 650 hPa circulation center, which are similar to the calculation of tilt and local shear vectors in *Rappin and Nolan* [2012]. These two vectors represent well the TC vortex tilt direction and magnitude, as well as the local shear felt by the TC vortex.

The time evolutions of the local vertical wind shear vectors and the storm-center tilt vectors of the selected members are examined in Figure 3 to understand when and how the three selected members start to differ systematically in both SH5 and SH6. The origins in Figures 3a and 3b are the 850 hPa centers; the point on the line is the 450 hPa center. In this interpretation, the precession and alignment process can be viewed clearly in one figure. The tilt vector of each ensemble member initially moves outward along the environmental downshear direction, while the local vertical shear vector is oriented to the right of the environmental shear as a combined result of the environmental shear and the additional shear component (There are two reasons for the additional shear component orienting to the right of the tilt vector. One is due to the shear-induced asymmetric circulation, which enhances the circulation along the tilt direction at the low levels. The other is due to the calculation method. Because we use the 650 hPa center as the center of the average circle, part of the high-level (450 hPa) and low-level (850 hPa) circulation may be outside the average circle, which will result in the additional local shear to the right of the tilt vector.) caused by the corresponding displacement of the low and high-level vortex centers (Figures 3c and 3d). During the first 24 h of the simulations, the members in the same ensemble set (that is, members with the same environmental wind shear) experience nearly identical evolutions of their tilt and local shear vectors. Systematic differences amongst members first appear in the tilt vector evolution after 30 h in both SH5 and SH6 (Figures 3a and 3b), immediately after the tilt vectors begin the precession process. In SH5, SH5-Early has a moderate tilt magnitude before 52 h; beyond this time, the tilt magnitude decreases to a value smaller than that of SH5-Medium and SH5-Late, and becomes the first member to finish precession and vortex alignment. Among the three selected members of SH5, SH5-Late has the largest tilt magnitude throughout its evolution. Moreover, the precessions of the tilt vectors progress steadily without reversing direction in these three SH5 members.

In SH6, SH6-Early has the smallest tilt magnitude and completes the precession process the fastest, with the tilt vector primarily rotating in the same direction (except for a brief reversal from day 4 to day 5, Figure 3b). In contrast, the tilt vectors of SH6-Medium and SH6-Late undergo more complicated precession processes, including numerous reversals in the direction of precession that lead to much longer times before the vortices become aligned. In addition, the tilt magnitudes of SH6-Medium and SH6-Late are generally larger than SH6-Early. The complicated tilt evolutions occur when the angle between the tilt vector and environmental shear vector ranges from 20° to 90° , during which time the convection cluster is drifting away from surface center. The local shear vectors evolve as a response to the changes in the tilt vectors, and are directed to the right of the tilt vector. It is quite obvious that the evolution of the tilt and shear vectors is much smoother and faster in SH5 than in SH6. The results in our idealized simulations display vortex alignment under precession, though the processes in real cases may be more complicated. For example, there could be reformation of the TC center in the area of intense convection to the downshear side [*Molinari et al.*, 2006, *Molinari and Vollaro*, 2010].

As is proposed in ZT13, we attribute the evolution differences between members within both SH5 and SH6 sets to the differences in the diabatic heating. Therefore, we examine in Figure 4 the azimuthally averaged column-integrated diabatic heating for the various ensemble members discussed above. The location and subsequent evolution of the radius of maximum azimuthally averaged 10 m tangential wind (RMW) is

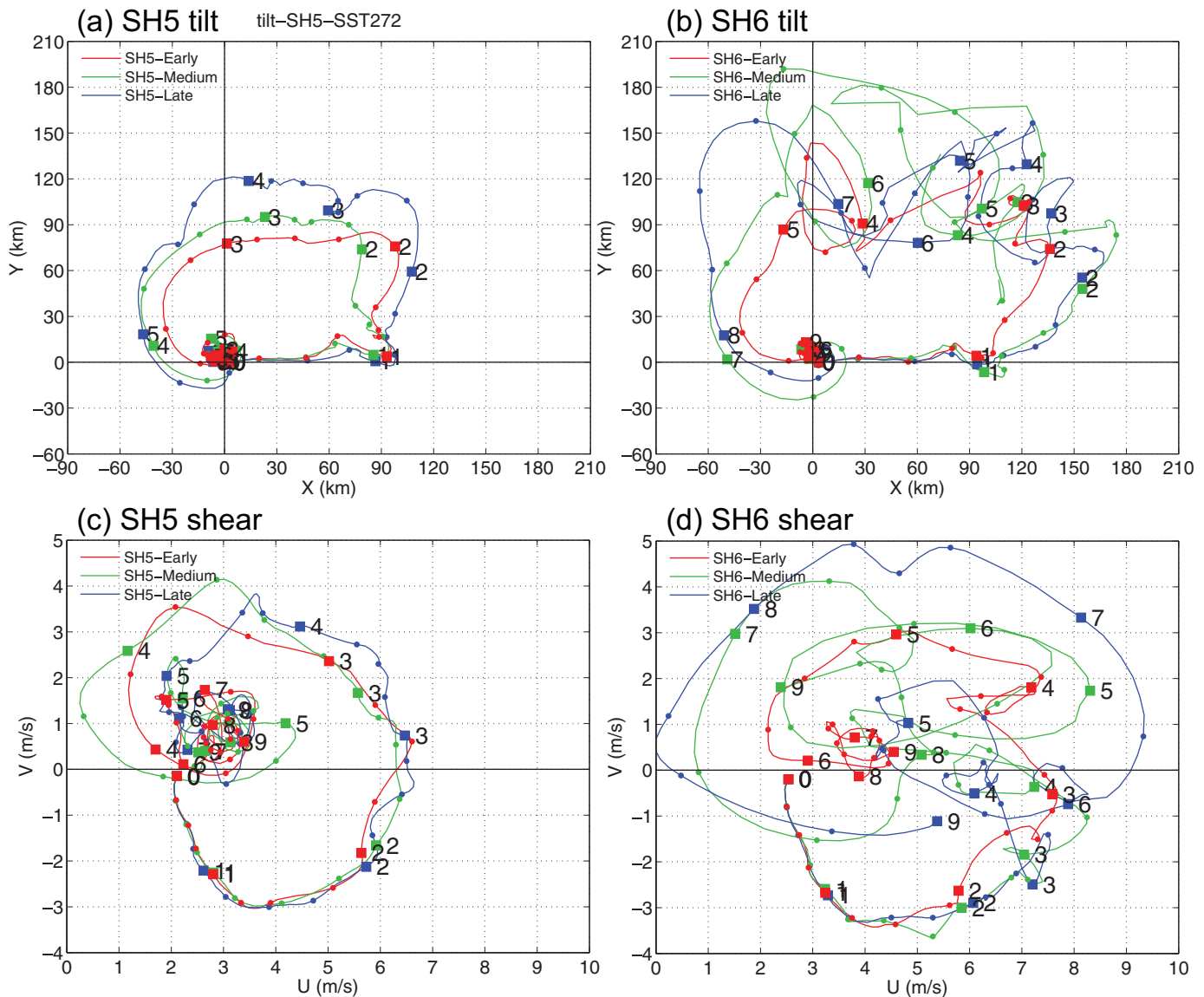


Figure 3. (a) Time evolution of tilt vectors under SH5; (b) the same as Figure 3a except for SH6; (c) time evolution of local shear vectors under SH5; (d) the same as Figure 3c except for SH6. Dot shows the 6 h interval and square shows 24 h interval. Numbers besides the squares show the simulation time in days.

closely related to the location of the convection; when the convection extends to larger radii, the RMW also becomes larger, which is reasonable because the location of the diabatic-heating-driven updraft is dominating the location of angular momentum convergence. For the SH5 members, SH5-Early has a generally continuous decrease in the RMW with only a slight increase at 48 h (Figure 4a), SH5-Medium has a slow trend of contracting RMW from 40 to 96 h (Figure 4b), while SH5-Late even experiences a period of increasing RMW from 72 to 108 h (Figure 4c). For the members in SH6, the RMWs experience larger oscillations over time before the final contraction of the primary circulation. SH6-Early contracts its strong convection within a radius of 120 km after 120 h (Figure 4d), while SH6-Medium finally succeeds in forming inner-core convection and subsequently reducing its RMW by 192 h (Figure 4e). SH6-Late has weak and sparse convection within a 120 km radius after 68 h and the RMW is therefore not able to contract due to the lack of effective strong convection close to the center until 156 h (Figure 4f). The main differences between the evolutions of the members in SH5 and SH6 result from the differences in the distribution of convection. The areas of convection in the SH5 members are more compact and temporally continuous whereas the areas of convection in the SH6 members are initially continuous in time but become sparser and extend far from the surface centers (out to 240 km) before RI onset. It is also important to note that each contraction of the

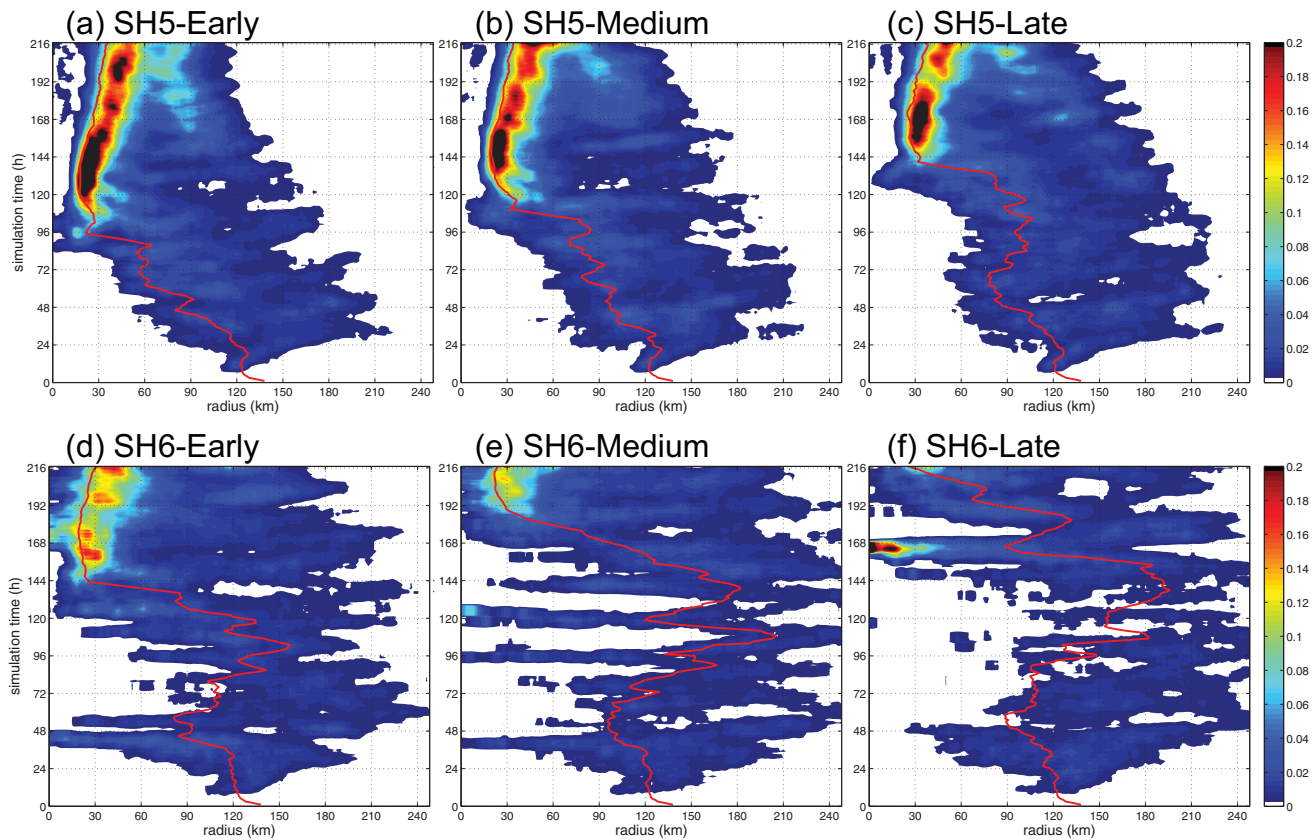


Figure 4. First row is the time evolution of azimuthally averaged column-integrated positive-only diabatic heating rate (K s^{-1}) for SH5 member, (a) SH5-Early, (b) SH5-Medium, and (c) SH5-Late. Second row is the same as first row except for SH6 member, (d) SH6-Early, (e) SH6-Medium, and (f) SH6-Late. Red line is the radius of maximum tangential wind.

RMW is accompanied by a convective burst within the RMW and close to the surface center. Though TZ14 already found that both the location and magnitude of diabatic heating are closely related to the TC vortex precession and alignment, the mean field cannot show the precession interruptions in SH6 caused by the temporary breakdown of the convection before the convection cluster reorganization.

To further illustrate how the convection evolves in SH6, Figure 5 shows the sea level pressure (SLP) along with the simulated column-maximum reflectivity in a $520 \text{ km} \times 520 \text{ km}$ box centered on the TC surface vortex at various times for each of the three selected members in SH6. At 24 h, under the influence of the 6 m s^{-1} westerly shear, the strongest convection is concentrated to the eastern (downshear) side, with no systematic differences in intensity between the members. At 48 h, the convective clusters have begun to show differences in location and intensity, with SH6-Late having weaker reflectivity values. By 108 h, the strongest convection in SH6-Early has crossed from the downshear-left quadrant into the upshear-left quadrant of the TC, while the strongest convection in both SH6-Medium and SH6-Late are still in the downshear-left quadrant and farther away from their surface centers. At 144 h, the convection in SH6-Early has wrapped around the center to become more axisymmetric; at this point, the minimum SLP of SH6-Early has become much lower than that of the other two members, and RI commences within a few hours. Meanwhile, the strongest convection in SH6-Medium has just moved to the upshear-left quadrant whereas convection of SH6-Late becomes poorly organized and remains in the downshear-left quadrant. By 168 h, SH6-Early has developed into a mature hurricane, while convection in SH6-Medium has just started to wrap around the center; at this same time, the strong convection cluster in SH6-Late has reorganized and is finally crossing from downshear-left to upshear-left—more than 60 h later than SH6-Early. If we compare Figure 5 here to SH5 in Figure 3 of TZ13, we can clearly see that, for all three members, SH5 has better-organized convective clusters with stronger maximum reflectivity values closer to the surface centers; this is also seen in TZ14 about the mean state of the ensembles (Figures 6a and 6b in TZ14).

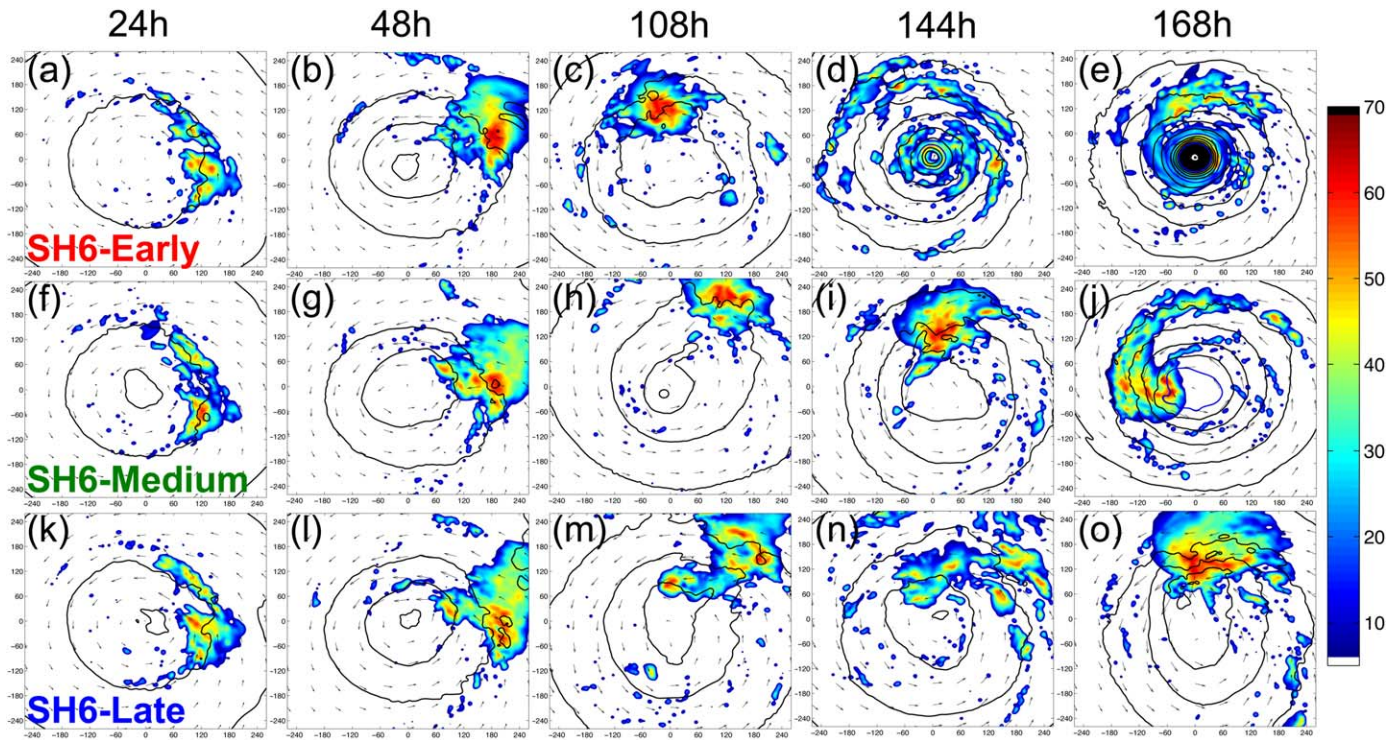


Figure 5. The 10 m surface wind vectors, sea level pressure (black contours every 2 hPa; thick blue contour for 1000 hPa), and column maximum reflectivity (dBZ; color filled) for ensemble members: (a–e) SH6-Early, (f–j) SH6-Medium, and (k–o) SH6-Late in SH6 at (from left to right) 24, 48, 108, 144, and 168 h.

5. Ensemble Sensitivity Analysis on Forecast Divergence and Error Growth Dynamics

In ZT13, we proposed that the divergence amongst the ensemble members under moderate environmental shear situation develops from the randomness of moist convection, and later leads to differences in the vortex primary circulation strength and hence the timing of precession and alignment. In order to further verify our hypothesis, correlations between related factors such as diabatic heating, tilt, RI onset time, and tangential wind are calculated for both the SH5 and SH6 experiments. Note that for a sample size of 20, a correlation of 0.5 is statistically different from 0 with roughly 95% confidence, while 0.7 is statistically different from 0 with roughly 99% confidence.

We show the temporal evolutions of the correlations between the column-integrated diabatic heating and the tilt magnitude (Figures 6a and 6d), RI onset time and column-integrated diabatic heating (Figures 6b and 6e), and between RI onset and azimuthally averaged 10 m tangential wind (Figures 6c and 6f). All of these radius-time correlation plots show regions of strong negative correlation closer to the center and regions of strong positive correlation farther from the center. This indicates that increased diabatic heating closer to (farther from) the vortex center leads to smaller (larger) tilt magnitudes (Figures 6a and 6d) and an earlier (later) onset of RI (Figures 6b and 6e); moreover, stronger tangential winds closer to (farther from) the center will result in an earlier (later) RI onset (Figures 6c and 6f).

From Figures 6a, 6b, 6d, and 6e, strong correlations between the diabatic heating and both tilt magnitude and RI onset time develop after 30 h in both SH5 and SH6, which is approximately the time after the first strong burst of convection. However, the relationships revealed by the correlations in the SH6 ensemble are not as strong as that in SH5. Generally speaking, diabatic heating is more strongly correlated with tilt magnitude than it is with RI onset, which is reasonable as the tilt responds directly to change of the diabatic-heating distribution and intensity. Although the correlation between the tangential wind and the RI onset time (Figures 6c and 6f) only becomes significant about 6 h after the initial strong burst of convection, this correlation is stronger and much smoother when compared to the diabatic heating correlations. The correlation structures are consistent with the hypothesis outlined in ZT13, where it was proposed that the tilt

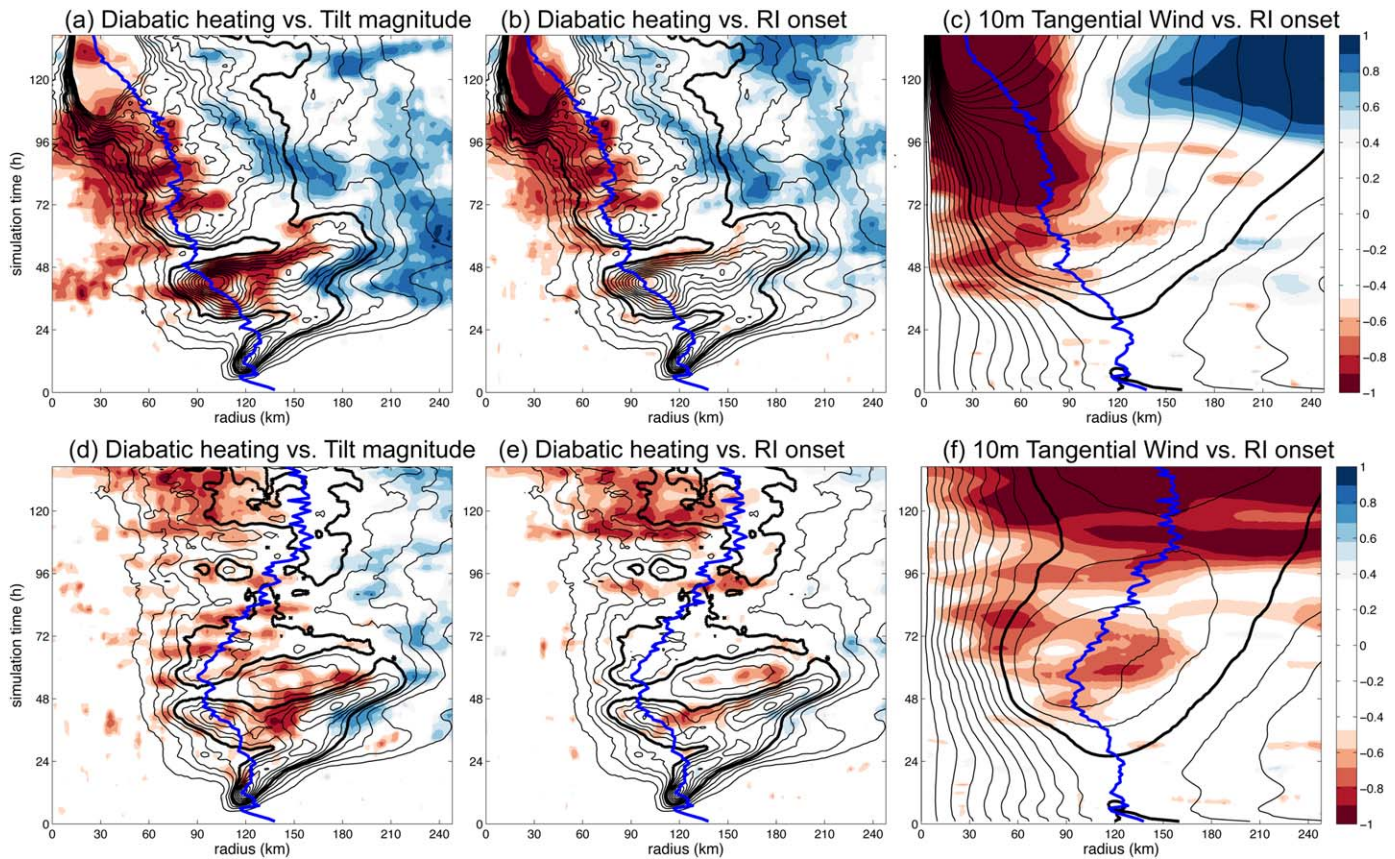


Figure 6. Radius-time plots. The black contours are the composite azimuthally averaged (a, b, d, and e) column-integrated diabatic heating (interval 0.002 K s^{-1} , thick black line for 0.01 K s^{-1}) and (c and f) tangential wind (interval 1 m s^{-1} , thick black line for 10 m s^{-1}). The blue thick line is the mean radius of maximum tangential wind. The shading is (a and d) correlation between diabatic heating and tilt magnitude at the same time, (b and e) correlation between diabatic heating and rapid intensification onset times, and (c and f) correlation between tangential wind and rapid intensification onset times. The shading is from -1 to 1 with 0.1 interval and small correlation (<0.5) masked out. First row for SH5 and second row for SH6. Contours are not showing the whole range in order to leave the shading clearer to be seen.

magnitude is highly correlated with the location and strength of the diabatic heating and that the primary circulation is very important to the precession speed and thus RI onset time. Regardless of which group of variables is more influential in determining the timing of RI onset, the correlation analysis reveals a complex relationship between the time of RI onset and the heating, tilt, and tangential wind in these simulations, which emphasizes the influence of these variables on the speed of TC development.

Figure 7 further illustrates the relationship between tilt and RI onset by showing the evolution of the correlation between the tilt vectors (magnitude and angle) and the RI onset times for the 20 members of SH5 and of SH6. The tilt magnitude is positively correlated with RI onset time, implying that larger tilt magnitudes lead to slower onsets of RI. The tilt angle, which can be used to represent the precession speed, is negatively correlated with the time of RI onset, so that members with larger tilt angles will tend to complete the precession process faster. During the first 24 h when the differences between the members in both SH5 and SH6 are very small and random, the strengths of the correlations steadily increase, which indicates that systematic differences are gradually developing. For SH5, the correlations between RI onset time and both tilt magnitude and angle become very strong as the members begin to approach RI. For SH6, however, the correlations have more fluctuations between 54 and 114 h as a result of the complex tilt evolution occurring during this period (Figure 3b), which in part stems from the difficulty in determining the midlevel vortex centers when the moist convection is more sparse and discontinuous (Figures 4 and 5). The strong correlation between tilt and RI onset time after tilt divergence in both ensemble sets are more evident for their relationship.

After the correlation analysis above, we see the lack of correlation in the first 30 h. Then, we are going to analyze how this initial random minute moisture error grows into the deterministic deviations using

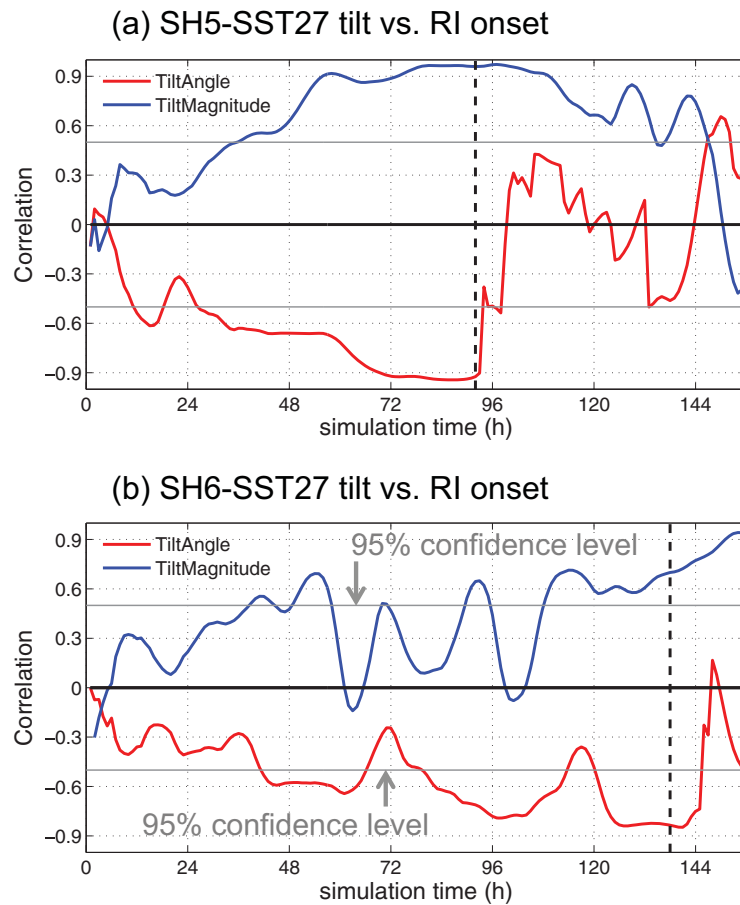


Figure 7. Time evolution of correlation coefficient between tilt vectors and RI onset times (a) SH5 and (b) SH6. Correlation values of 0.5 are marked to denote the 95% level for statistical significance; the zero correlation line is also drawn.

difference kinetic energy (DKE) between SH5-Early and SH5-Late and its 2-D spectrum analysis (Figure 8). DKE is defined as

$$DKE = \frac{1}{2} \sum \rho [(\delta u)^2 + (\delta v)^2 + (\delta w)^2], \quad (1)$$

where ρ is the mean density and $\delta(u, v, w)$ are the differences in the (u, v, w) velocity components between the two members at each grid point. Figures 8a–8d show DKE at different times with summation only in the vertical layers. From 24 to 106 h, the DKE field expands from only the convective area (Figures 8a and 8b) to the entire storm range (Figures 8c and 8d) (the comparison of these two members is in Figure 3 of ZT13). In order to separate the DKE in different scales, the 2-D spectral decomposition is computed using the Fast Fourier Transform (FFT) algorithm following *Zhang et al.* [2002, 2003, 2007]. First, FFT is performed for δu , δv , and δw at each vertical level, and then the DKE at each scale is calculated at each point and finally summed up throughout the entire inner domain grid points. Figure 8e plots DKE at three different scales (DKES: convective scale $L < 50$ km; DKEM: storm inner-core scale $50 < L < 300$ km; DKEL: entire storm scale $L > 300$ km). We find that DKES first starts to increase at about 10 h. After about 40 h DKES saturates to a near-constant value, at which time the growth of medium scale difference (DKEM) becomes dominant. This is again telling us that the differences between SH5-Early and SH5-Late first start to grow from small-scale moist convection and then accumulates to the systematic deviation at the vortex inner-core scale before finally impacting the balanced mean circulation.

The dependence of RI predictability on different TC stages is also explored by adding five sets of moisture perturbations to the unperturbed 5 m s^{-1} -shear simulation at different times (24, 48, and 72 h, denoted by SH5-day1, SH5-day2, and SH5-day3, respectively). The maximum 10 m winds and corresponding standard

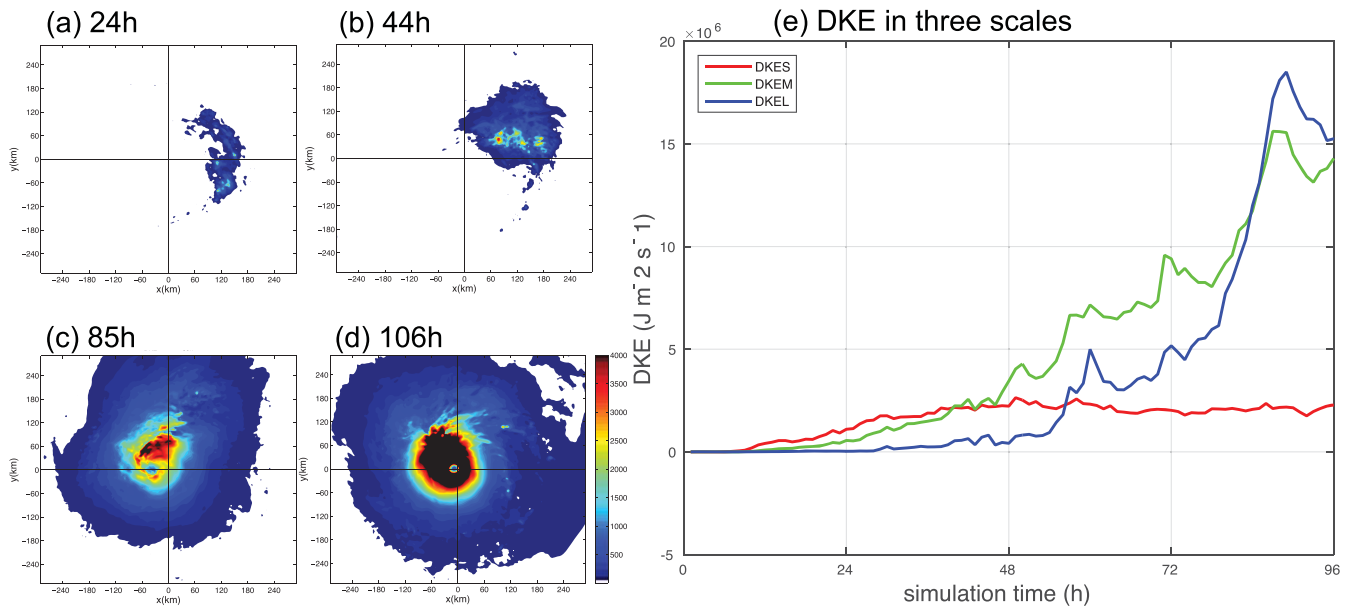


Figure 8. Different kinetic energy (DKE, $\text{kg m}^{-1} \text{s}^{-2}$) between member SH5-Early and SH5-Late in SH5 at (a) 24 h, (b) 44 h, (c) 85 h, and (d) 106 h. (e) Time evolution of DKE in three scales: DKES < 50 km < DKEM < 300 km < DKEL.

deviations are shown in Figure 9. The five SH5-day1 ensembles have similar standard deviation pattern as SH5 while SH5-day2 and SH5-day3 are developing with very small spread in RI onset time (Figure 9b). It is suggesting that at the very beginning stage (the stage of asymmetry formation), the randomness of convection is able to adjust the extent of asymmetry; while at later stages, the randomness of convection is not able to distract the development after the dominant feature of major convection cluster forms after 30 h which is the time of occurrence of high correlations (Figures 6a–6c).

As a brief summary of this section, we see that the correlations with vortex tilt and RI onset are small and random over the first 30 h, which is consistent with the spectrum analysis that shows DKE growth is mainly at the convective scale during this period. From the correlation of diabatic heating and tilt, we know that

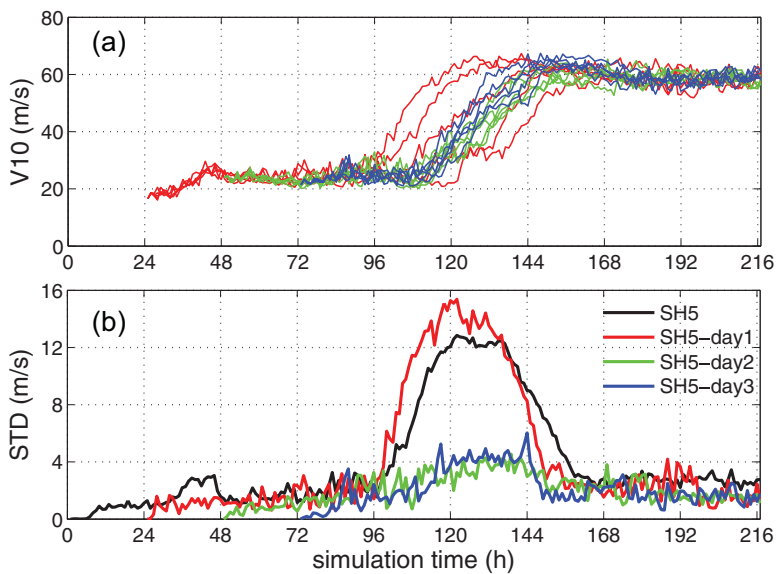


Figure 9. (a) Time evolution of the tropical cyclone intensity in terms of the 10 m maximum wind speed for SH5-day1, SH5-day2, and SH5-day3; (b) standard deviation of maximum 10 m wind for SH5, SH5-day1, SH5-day2, and SH5-day3.

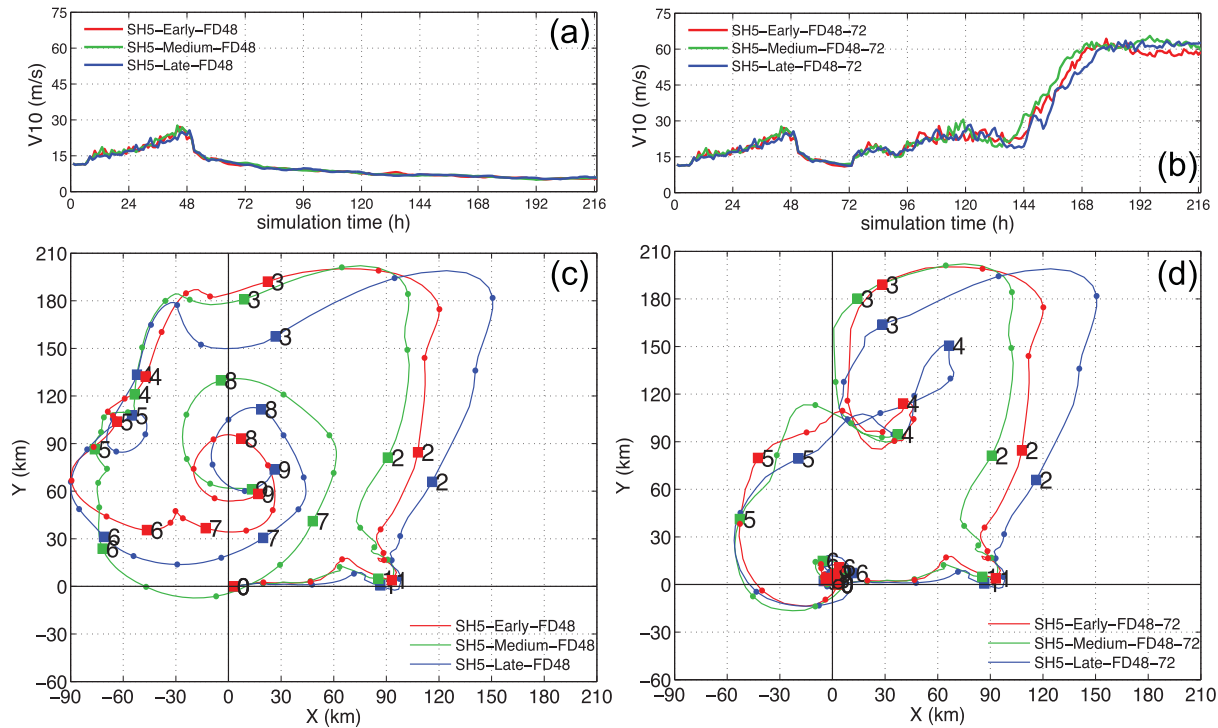


Figure 10. Fake-dry experiments of three typical members in SH5. (a and c) FD48: fake dry starts from 48 h to the end of the simulation; (b and d) FD48-72: fake dry only during 48–72 h. (a and b) Time evolution of maximum 10 m wind; (c and d) time evolution of tilt vectors.

both the intensity and location of the moist convection affect the tilt magnitude/alignment process. In our initial vortex and environmental setup, when the shear approaches a certain critical magnitude (between 6 and 7.5 m s^{-1}) above which the environment will become too hostile for TC development, the convection becomes disorganized and discontinuous both spatially and temporally, resulting in weak correlations (Figures 6d, 6e, and 7b). In contrast, the correlation between RI onset time and the mean vortex circulation is smoother and more continuous. Errors (as measured by DKE) are found to grow from the convective scale up to TC-related mean circulation scale, exhibiting how and when the randomness in moist convection accumulates to influence the predictability of RI. The sensitivity experiment of adding perturbation at different times reveals that the predictability of TC is depending on its development stages.

6. Fake-Dry Experiments

In this section, another two sets of “fake-dry” sensitivity experiments are conducted to explore the role of diabatic heating (due to water phase changes) on the precession. Using the three typical members in SH5 (SH5-Early, SH5-Medium, and SH5-Late) as control simulations, the suffix “FD48” denotes the sensitivity set in which diabatic heating is turned off after 48 h while “FD48-72” denotes the set in which diabatic heating is only turned off between 48 and 72 h. The maximum 10 m wind decreases immediately after turning off the diabatic heating (Figures 10a and 10b) because of the decay of the secondary circulation (Figure 11b). The maximum 10 m wind increases to right after diabatic heating is turned back on at 72 h and the TC’s secondary circulation is restored (Figure 11c). The tilt vectors of all three members in FD48 (Figure 10c) undergo precession and alignment similar to the dry dynamics of the Vortex Rossby Wave (VRW) damping described in *Reasor et al.* [2004], such that the vortices tend to achieve steady state tilts ($\sim 80 \text{ km}$) to the left of the environmental vertical wind shear vector and the tilt magnitudes cannot keep small values ($< 10 \text{ km}$) as in Figure 3a. For FD48-72, all three members experience a sharp decrease in tilt magnitude after diabatic heating is turned back on at 72 h (Figure 10d); when the tilt magnitudes reach their minima ($< 10 \text{ km}$), RI begins with a much smaller spread in onset time ($\sim 6 \text{ h}$) (Figure 10b) amongst the three members than in the corresponding control runs (Figure 2c).

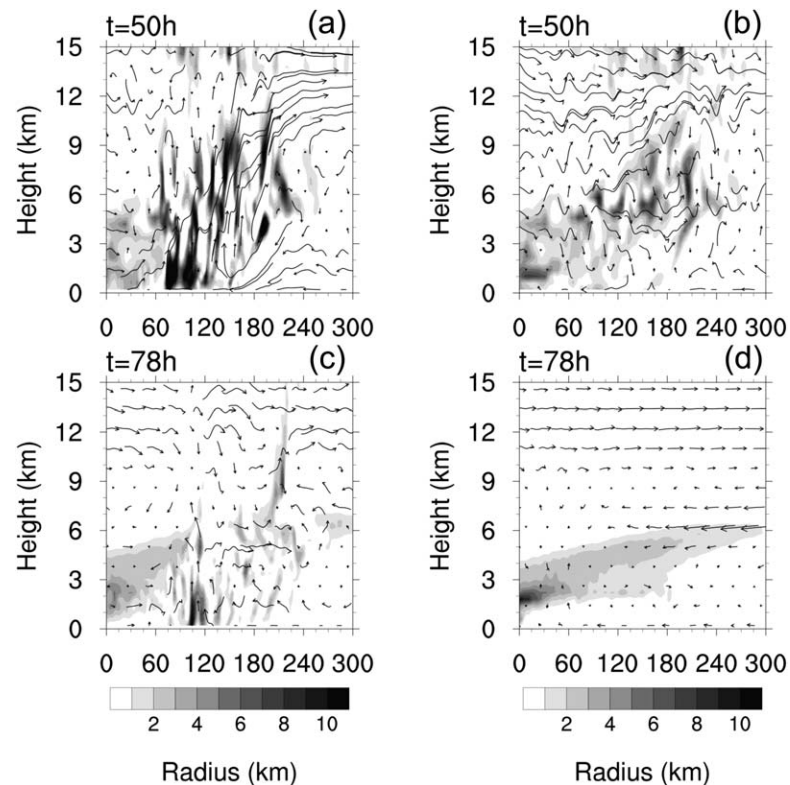


Figure 11. Cross section of density-weighted PV ($10^{-6} \text{ K m}^{-1} \text{ s}^{-1}$, shading) and secondary circulation (m s^{-1} , vertical velocity is 10 times larger, curly vectors) along tilt direction through the surface center. (a) SH5-Early at 50 h along 40° angle to the left of environmental shear; (b) SH5-Early-FD48 at 50 h along 40° angle to the left of environmental shear; (c) SH5-Early-FD48-72 at 78 h along 84° angle to the left of environmental shear; (d) SH5-Early-FD48 at 78 h along 92° angle to the left of environmental shear.

In order to have a closer look at the vortex column evolutions in the control and fake-dry experiments (we use SH5-Early as an example because the other two have similar behavior), we plot cross sections of density-weighted potential vorticity (PV) for SH5-Early, SH5-Early-FD48, and SH5-Early-FD48-72 (Figure 12). At 50 h, SH5-Early-FD48 still has similar PV and equivalent potential temperature θ_e patterns as SH5-Early, except the diabatic heating induced PV on the down-tilt side is not seen (Figure 12d). At later times (60 and 72 h), the vortex column of SH5-Early-FD48 becomes more tilted and the low-level vortex gradually decays because the secondary circulation diminishes (Figure 11b) and there is nothing to counteract the effect of surface friction. Meanwhile, the mid and high-level vortices can persist with almost no decay in strength for a long time. During this period, SH5-Early intensifies and precesses faster. After turning on the diabatic heating, SH5-Early-FD48-72 resumes some weak convection at first and quickly recovers its surface vortex (Figures 12g–12i), while SH5-Early-FD48 continues weakening (Figures 12j–12l).

Through these sensitivity simulations, we find that the secondary circulation driven by diabatic heating from moist convection is important for vortex alignment. Without diabatic heating, the vortex column can continue precessing and aligning, which *Reasor et al.* [2004] attribute to a dry inviscid VRW damping mechanism; however, this alignment is not as complete as the one in SH5-Early (with diabatic heating). For simulations in which diabatic heating is turned back on at 72 h, the differences between members do not grow much, indicating that the error growth needs the existence of diabatic heating during the critical period (when the tilt angle is between 20° and 90° to the left of the environmental shear vector) as well as time to accumulate.

7. Intrinsic Versus Practical Limits of Predictability

By chance, we found that even tiny numerical precision errors due to the use of different computational architecture can lead to large differences in TC development, which is also found in *Hong et al.* [2013]. Using

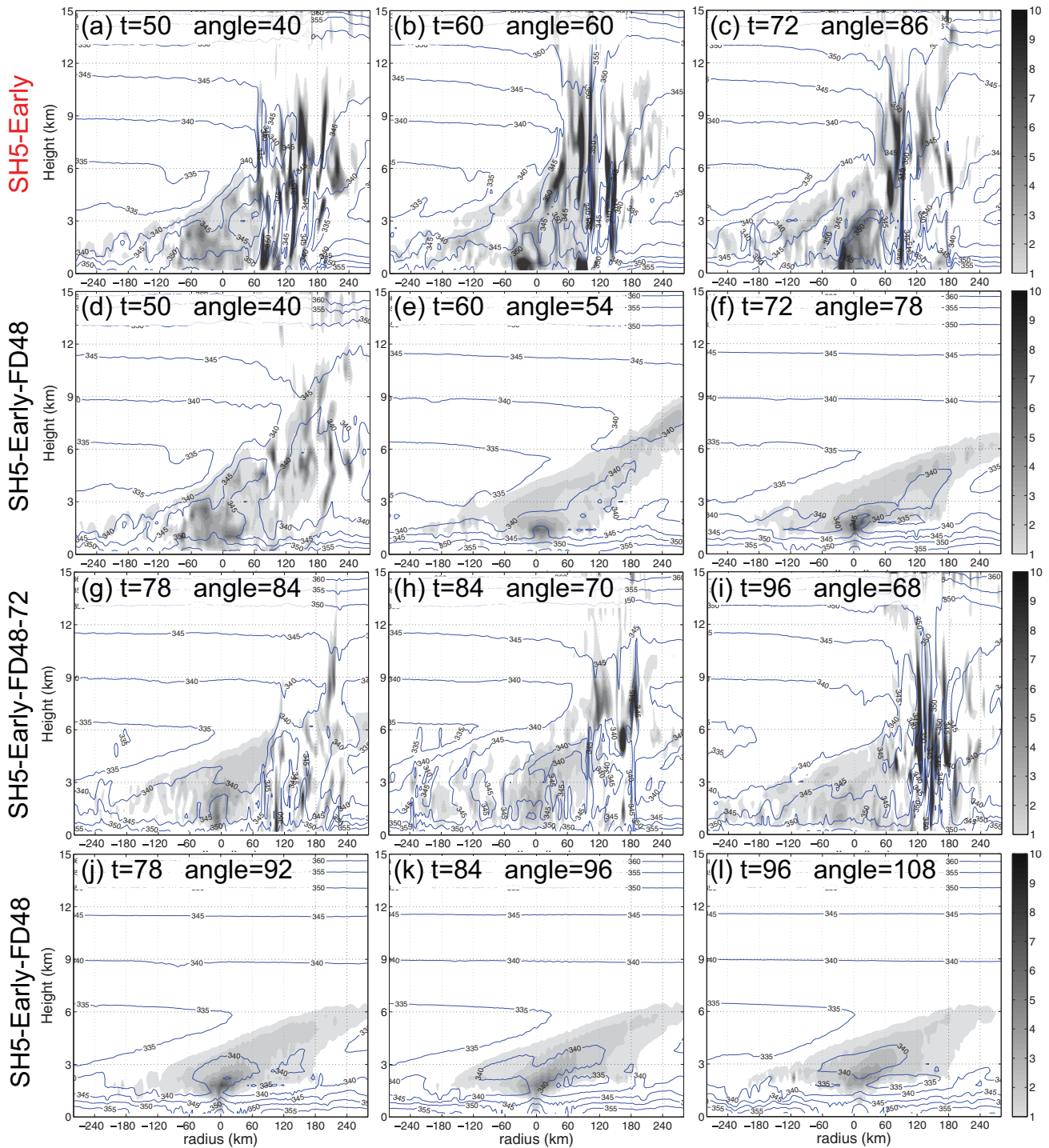


Figure 12. Cross section of density-weighted PV ($10^{-6} \text{ K m}^{-1} \text{ s}^{-1}$, shading) and θ_e (K, contour) along tilt direction through the surface center. Time (50, 60, 72, 78, 84, and 96 h) and angle to the initial environmental shear are shown. (first row) Control member SH5-Early, (second row) SH5-Early-FD48, (third row) SH5-Early-FD48-72, and (fourth row) SH5-Early-FD48.

exactly the same initial conditions and model setups, the SH5 ensemble set was run on two supercomputers at the Texas Advanced Computing Center (TACC): Ranger (Figure 13a), which has since been retired and replaced by Stampede (Figure 13b). Some individual members exhibit substantial differences between the two computers: for example, ensemble member EN14 (EN24) underwent RI 1 day earlier (later) on Stampede than the same member on Ranger (Figure 13). In this case, we see that the predictability is intrinsically limited under shear of 5 m s^{-1} . It is rather troubling that a single simulation cannot be closely replicated

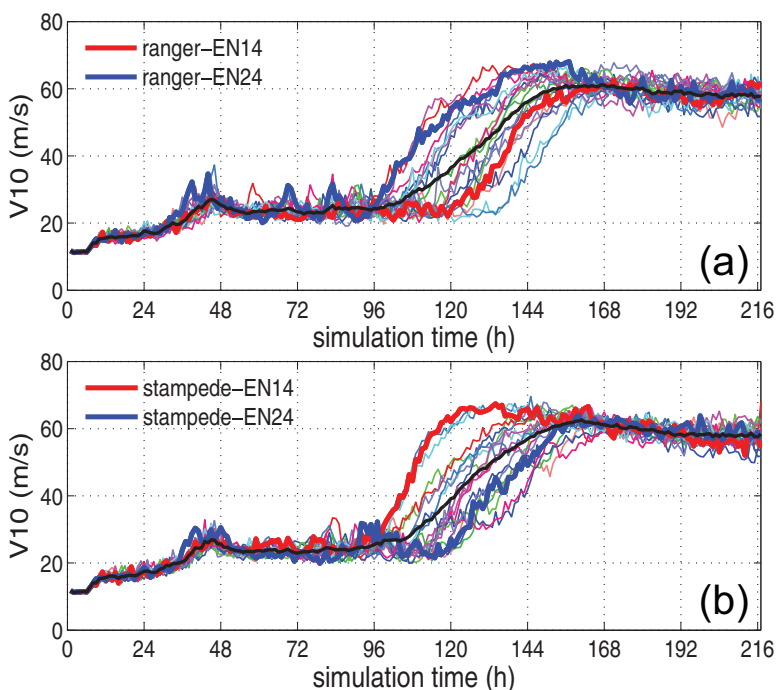


Figure 13. Time evolution of the tropical cyclone intensity in terms of the 10 m maximum wind speed for (a) SH5 on ranger and (b) SH5 on stampede.

under slightly different computing architecture. Fortunately, the evolution of the ensemble mean is quite similar for both computers, highlighting the merits of using ensemble-based probabilistic forecasts.

To further compare intrinsic predictability with practical predictability, we generate two sets of 20-member ensembles by randomly sampling shear magnitudes from normal distributions with a mean of 6 m s^{-1} : one set is from a distribution with a standard deviation of 0.1 m s^{-1} (SH6-STD0.1), while the other has a standard deviation of 0.5 m s^{-1} (SH6-STD0.5). The shear magnitudes and RI onset times for all members of both sets are listed in Table 1. Examination of Figures 14a and 14b shows that with greater variation in shear (standard deviation 0.5 m s^{-1}), the spread of RI onset times can be as large as 4 days, while with smaller variation in shear (standard deviation 0.1 m s^{-1}), the spread is similar to that of SH6. In Table 1, we see that the nondeveloper EN29 in SH6-STD0.1 has the largest shear magnitude of 6.2753 m s^{-1} , while member EN16—with only 0.02 m s^{-1} less shear—starts RI at 172 h. In this set, we also find that the earliest developer (EN17) is not the one with smallest shear magnitude (EN22). Moreover, member EN26 with shear of 6.1099 m s^{-1} develops 32 h earlier than member EN24 with shear of 5.8915 m s^{-1} (Figure 14a). At the same time, in SH6-STD0.5, the members with the largest shear values do not have TC development whereas the members with the smallest shear values develop TCs the earliest (Table 1). The correlation coefficient between environmental vertical wind shear and RI onset time for SH6-STD0.1 is 0.431 with a p -value of 0.0578 while for SH6-STD0.5 the correlation is 0.806 with a p -value of nearly zero, which shows that for SH6-STD0.5, the members with larger shear magnitudes are more likely to develop later (if at all).

The correlation between environmental shear magnitudes and maximum 10 m winds at each simulation time is calculated for SH6-STD0.1 and SH6-STD0.5 (Figure 14c). Both sets show negative correlation, meaning stronger shear corresponds to weaker TC intensity. What is important here is that SH6-STD0.1 almost never has a statistically significant correlation, whereas SH6-STD0.5 has a statistically significant correlation (95% confidence) after ~ 60 h. This is consistent with the correlations between shear magnitude and RI onset time discussed in the previous paragraph: for a larger spread in shear magnitudes, vortex development is more predictable (as a function of shear), which is in the regime of practical predictability since the large-scale environmental shear to the accuracy of $\sim 1 \text{ m s}^{-1}$ can be promisingly achieved by assimilating more observational data.

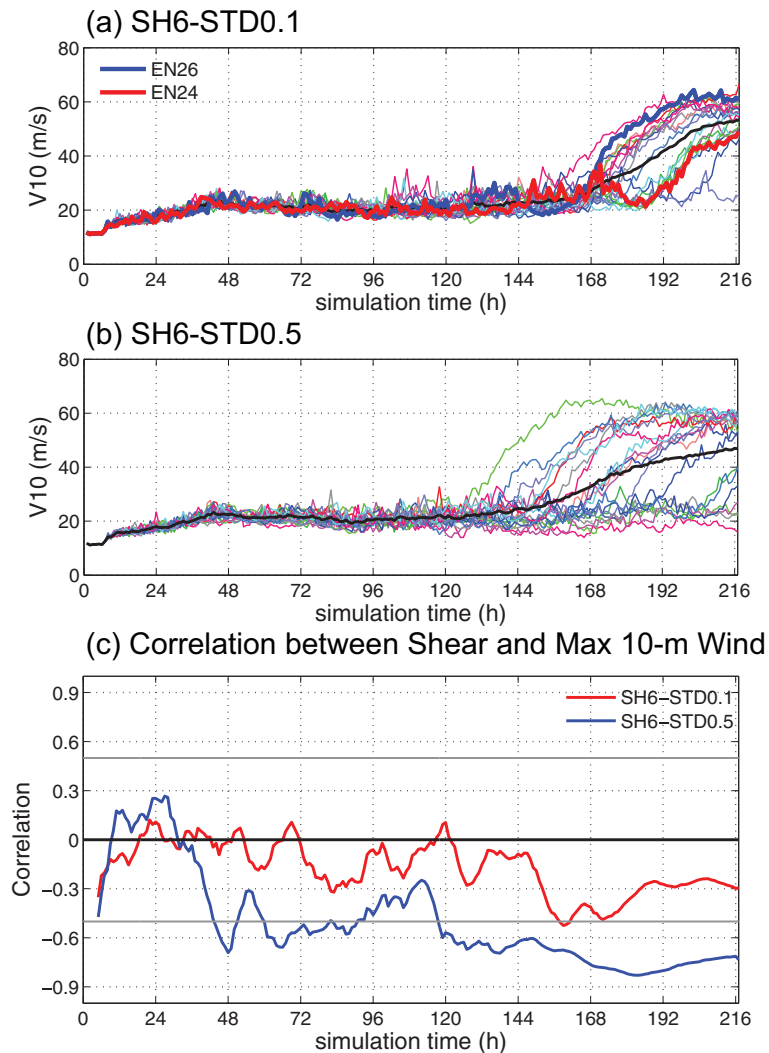


Figure 14. Time evolution of the tropical cyclone intensity in terms of the 10 m maximum wind speed for the ensemble set of (a) perturbed shear with standard deviation of 0.1 m s^{-1} and (b) perturbed shear with standard deviation of 0.5 m s^{-1} . (c) Correlation between the initial shear magnitude and in situ maximum 10 m wind in both sets. Grey horizontal line indicates 95% confidence level.

The temporal evolutions of the correlation between the column-integrated diabatic heating and the tilt magnitude (Figures 15a and 15d), as well as the correlations between RI onset time and both column-integrated diabatic heating (Figures 15b and 15e) and azimuthally averaged 10 m tangential wind (Figures 15c and 15f) are shown. The mean fields of azimuthally averaged diabatic heating and tangential wind of both sets are similar to Figures 6d and 6f. As in section 5, regions of strong negative (positive) correlation are found closer to (farther from) the center. This indicates that more diabatic heating located closer to the vortex center leads to smaller tilt magnitudes whereas more diabatic heating located farther away from the vortex center leads to larger tilt magnitudes (Figures 15a and 15d), which is the case regardless of sampling standard deviation (we can treat SH6 as a standard deviation of 0 m s^{-1}). Furthermore, the correlation between RI onset time and diabatic heating in SH6 (Figure 6e) is comparable to or even slightly weaker than in SH6-STD0.5 (Figure 15e), but is noticeably stronger than the correlation in SH6-STD0.1 (Figure 15b).

From TZ14, we know that the ensemble-mean vortex tilt magnitude is a function of shear (Figures 3a and 3b in TZ14) although there is also variability amongst ensemble members with the same shear (Figures 3a and 4b). The effect of shear and the randomness of convection can work together to affect the distribution of convection and hence vortex tilt. To further illustrate the relation between tilt and RI onset, Figure 16 shows the evolution of the correlations between the current tilt vector (magnitude and angle) and the RI

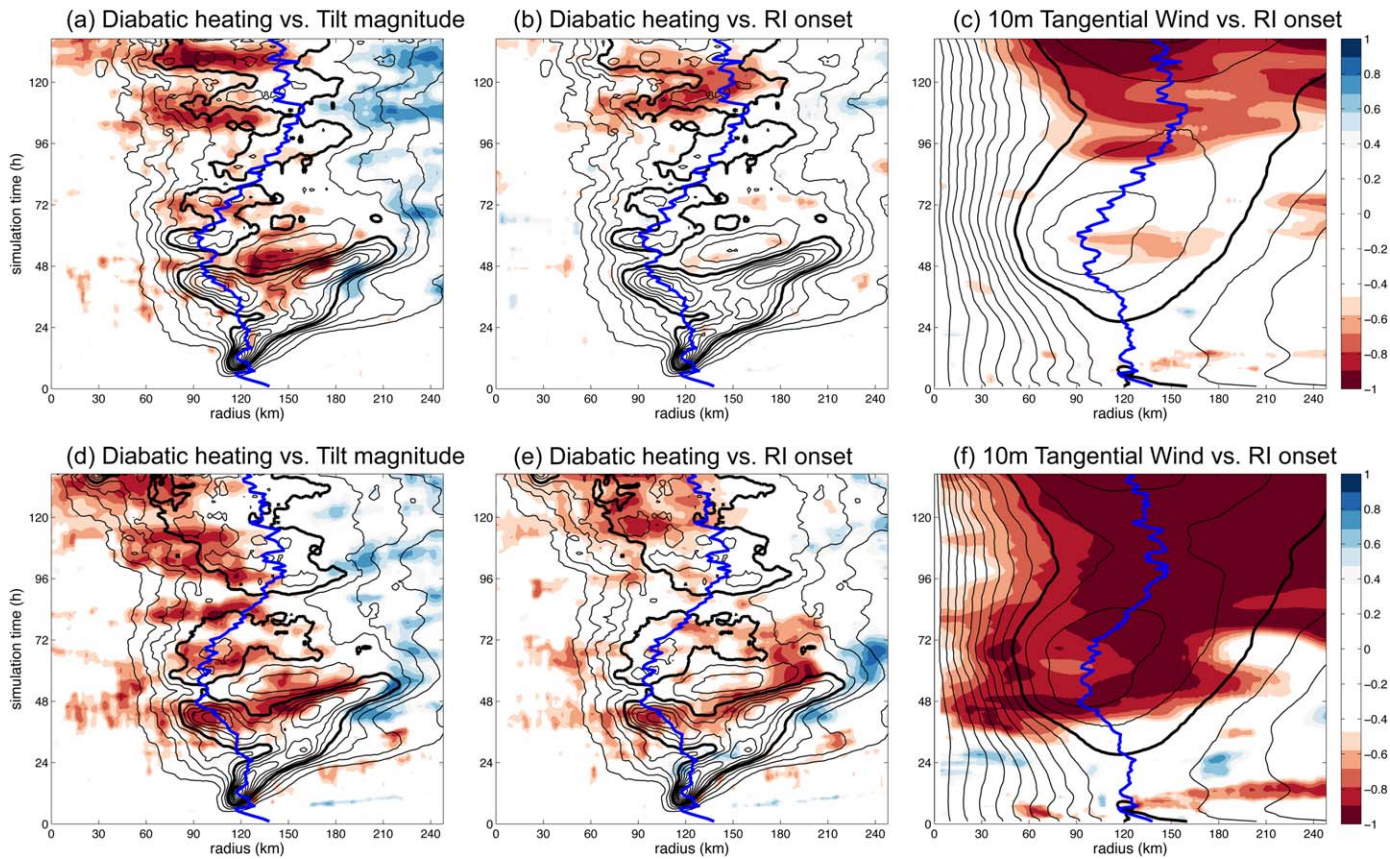


Figure 15. Radius-time plots. The black contours are the composite azimuthally averaged (a, b, d, and e) column-integrated diabatic heating (interval 0.002 K s^{-1} , thick black line for 0.01 K s^{-1}) and (c and f) tangential wind (interval 1 m s^{-1} , thick black line for 10 m s^{-1}). The blue thick line is the radius of maximum tangential wind. The shading is (a and d) correlation between diabatic heating and tilt magnitude at the same time, (b and e) correlation between diabatic heating and rapid intensification onset times, and (c and f) correlation between tangential wind and rapid intensification onset times. The shading is from -1 to 1 with 0.1 interval and small correlation (<0.5) masked out. (first row) SH6-STD0.1 and (second row) SH6-STD0.5. Contours are not showing the whole range in order to leave the shading more clear to be seen.

onset time for both the SH6-STD0.1 and SH6-STD0.5 ensembles. For SH6-STD0.1 (Figure 16a), the correlations are not straightforward and vary considerably throughout the time before the earliest onset of RI. In contrast, the correlation between tilt magnitude and RI onset time for SH6-STD0.5 (Figure 16b) is quite large (>0.6) during the first 48 h. This indicates that a more tilted vortex takes a longer time to start RI. Initially, the tilt of the vortex column is largely determined by the shear magnitudes in SH6-STD0.5 given the larger spread in shear magnitudes of the members. This correlation is weakened once the members precess into the area of large convective uncertainty (tilt angle between 20° and 90°), as is the case in SH6 (Figure 3b). At all times, RI onset is more strongly correlated with tilt angle than with tilt magnitude.

Though the intrinsic predictability of TCs is ultimately limited under moderate to strong environmental shear due to the chaotic nature of moist convection, we do see the high sensitivity of TC intensity to small vertical wind shear magnitude differences, which is also consistent with the findings by Moskaitis [2010]. The strong correlation between shear magnitude and the time of RI onset for SH6-STD0.5 indicates that there is still room for improving TC intensity forecasts through more accurate estimation of environmental shear.

8. Discussion and Conclusions

This study further explores the effect of vertical wind shear on the predictability of TC RI onset through cloud-resolving ensemble simulations using the Weather Research and Forecasting (WRF) model. Deep-layer shear magnitudes of up to 10 m s^{-1} are explored. The predictability of TC genesis is largely dependent on the hostility of the environment to the TC development. It is interesting to note that the ventilation

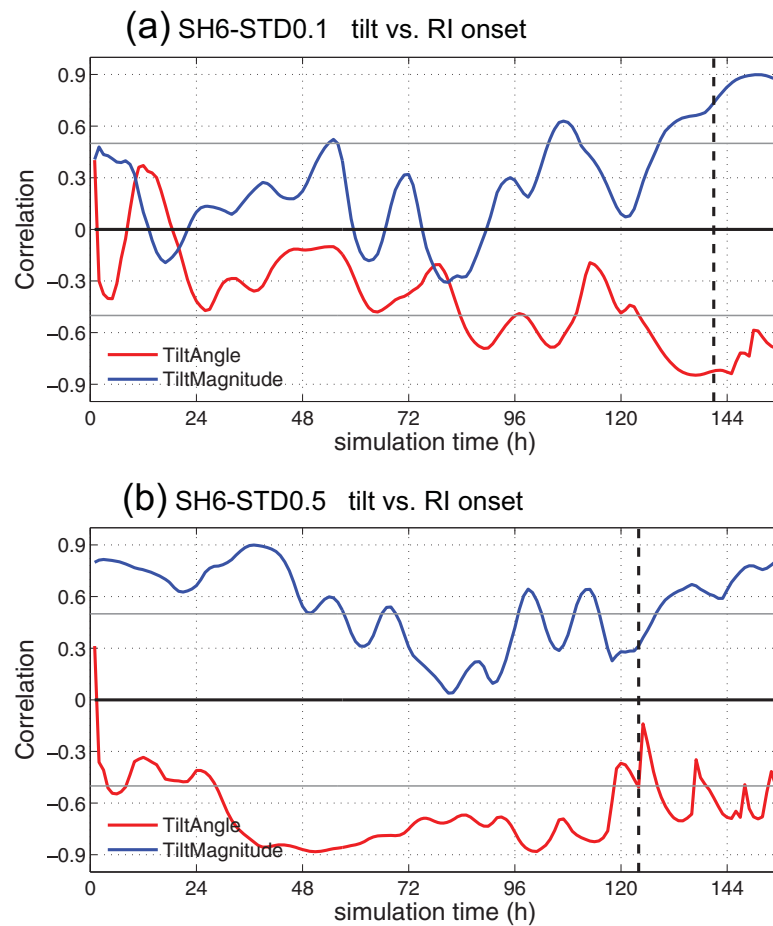


Figure 16. Time evolution of correlation coefficient between tilt vectors and RI onset times (a) SH6-STD0.1 and (b) SH6-STD0.5. Dash line represents the time for earliest RI onset. Grey horizontal line is 95% confidence level.

index (VI) [Tang and Emanuel, 2012] calculated from the initial conditions used in our simulations (Table 2) closely mirrors the spread in RI onset time. Specifically, the spread in RI onset time increases with VI, until extremely hostile conditions (SH7.5 and SH10, with $VI \geq 0.05$) prevent TC development.

The influence of the adverse environment can only happen when the TC is vulnerable (e.g., large tilt) and the TC could be near the point of bifurcation (develop or not). Due to the hostile effect of tilting the vortex column and driving away the convection, larger magnitudes of vertical wind shear lower the predictability of RI onset. Our study also shows that initially unobservable differences in low-level moisture propagate upscale through the randomness of convection (Figure 8) to yield considerable spread in the RI onset time. This randomness of moist convection first changes the TC structure subtly, then affects the storm-scale convective distribution before finally altering the strength of the storm's primary circulation, which could influence the resistance of the vortex to the environmental shear. After the systematic difference builds up, the following TC development is mostly dominated by the state of the TC vortex, which is consistent with the studies by Moskaitis [2010] and Torn and Cook [2013] that the evolution of TC vortex is highly sensitive to its initial intensity and structure (in our case, we can treat the time of the systematic difference occurrence (~ 30 h) as the "initial time"). Generally speaking (besides the set of SH6-STD0.1), Figure 17 can explain how moist convection can adjust the precession and alignment speed at later stages. Given the existence of this systematic difference, if the main cluster of moist convection is close to the center, the efficiency of converting diabatic heating (due to phase changes of water) into primary circulation kinetic energy is high, and the tilt will decrease (Figure 17a). When the main cluster of moist convection is farther from the center, the efficiency of converting diabatic heating to primary circulation kinetic energy is lower, and the tilt will increase in this case (Figure 17b),

Table 2. Ventilation Index for Different Environmental Conditions at Initial Time^a

Environmental Conditions	Ventilation Index
SH1	0.0067
SH2.5	0.0167
SH5	0.0334
SH6	0.0400
SH7.5	0.0500
SH10	0.0667

^aRed ones cannot develop; blue one can develop but with large uncertainty of RI onset time.

consistent with recent studies of Wang [2009] and Fudeyasu and Wang [2011]. When the shear is large, the convection and the vortex primary circulation are weak before alignment, which leads to a stagnation of the precession process. In this case, variations in both the distance from center and intensity of moist convection have a great impact on the timing of TC precession.

In TZ14 about the mean state of the ensemble simulations, it is the shear that initially dominates the tilt magnitude (which is quite similar to SH6-STD0.5 of this manuscript). In the present study, we also see that the small moisture errors that are initially present in the

boundary layer first manifest in the randomness of moist convection and then generally accumulate over time to influence the entire TC vortex, eventually leading to dramatic differences in the RI onset time—particularly as the shear magnitude approaches a certain critical value (SH6 in Figure 2d). Even in the moderate shear case (SH5), tiny changes to the numerics of computing architecture can lead to differences in the timing of RI onset of as large as 1 day. Such limited predictability happens in the presence of convective diabatic heating. The “fake-dry” experiments that turned off phase-change-induced diabatic heating demonstrate that moist convection is not only important for the accumulation/growth of errors over time, but also necessary to fully align the vortex column.

The transition from the issue of intrinsic predictability (small, random differences in moisture) to that of practical predictability (noticeable differences in environmental shear) described in section 7 gives us an idea that given the large errors in large-scale environmental factors (e.g., shear in our case), forecasts of TC intensity remain problematic, but can be improved by reducing the observational errors to the state of the art [Emanuel et al., 2004]. However, given the accurate environmental conditions, the predictability of RI is strongly controlled by internal dynamical processes, which are intrinsically limited by the randomness of moist convection. As stated in Melhauser and Zhang [2012], the predictability of a nonlinear system is also highly related to the current dynamic regime. If the dynamic system is in a regime of high predictability (e.g., the weaker shear of SH2.5), then reducing errors in the initial and boundary conditions can significantly increase forecast skill, and thus an issue of practical predictability. On the other hand, if the dynamic system is around the regime transition period (e.g., the moderate to strong shear of SH5 and SH6), forecast errors can remain large even with unnoticeable tiny initial differences from the truth, in which case the predictability is limited in intrinsic sense.

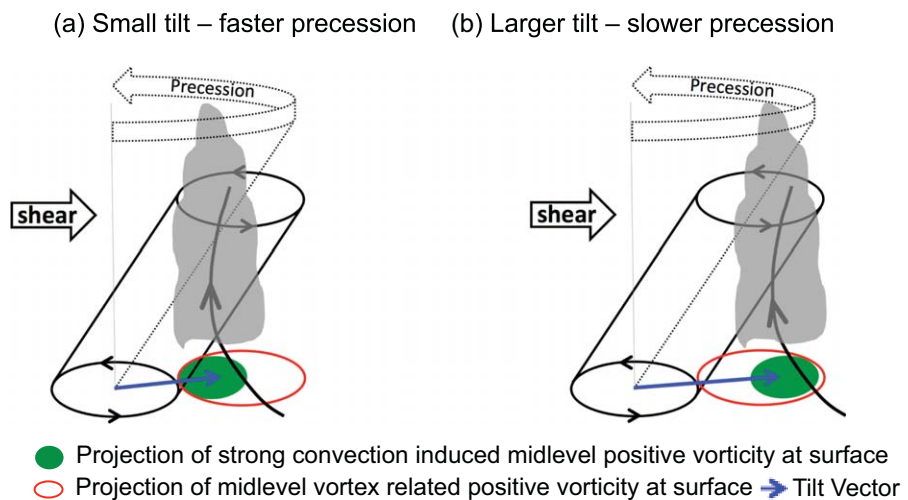


Figure 17. (a and b) Diagrams of how convection influence the tilt of the TC vortex. Given a tilted vortex, (a) if the convection is closer to the surface center, the tilt will become smaller; (b) if the convection is far from the surface center, the tilt will become larger.

Acknowledgments

This work is partially supported by NASA under grant NNX12AJ79G, NOAA HFIP, and by the Office of Naval Research under grant N000140910526. The authors are grateful to Daniel Stern and Dave Nolan for providing the code to add vertical wind shear. The authors benefit greatly from discussions with and/or comments from Kerry Emanuel, Rich Rotunno, Jenni Evans, Yevette Richardson, Erin Munsell, and Ben Green. Computing is performed at TACC. The WRF simulation data used in this study are archived in the TACC storage facility, and can be made freely available upon request.

References

- Chen, S. S., J. A. Knaff, and F. D. Marks Jr. (2006), Effects of vertical wind shear and storm motion on tropical cyclone rainfall asymmetries deduced from TRMM, *Mon. Weather Rev.*, *134*, 3190–3208.
- Davis, C. A., and D. A. Ahijevych (2012), Mesoscale structural evolution of three tropical weather systems observed during PREDICT, *J. Atmos. Sci.*, *69*, 1284–1305.
- Davis, C. A., S. C. Jones, and M. Riemer (2008), Hurricane vortex dynamics during Atlantic extratropical transition, *J. Atmos. Sci.*, *65*, 714–736.
- DeMaria, M. (1996), The effect of vertical shear on tropical cyclone intensity change, *J. Atmos. Sci.*, *53*, 2076–2087.
- DeMaria, M., and J. Kaplan (1999), An updated Statistical Hurricane Intensity Prediction Scheme (SHIPS) for the Atlantic and Eastern North Pacific Basins, *Weather Forecast.*, *14*, 326–337.
- Dunion, J. P. (2011), Rewriting the climatology of the tropical North Atlantic and Caribbean Sea atmosphere, *J. Clim.*, *24*, 893–908.
- Emanuel, K. A. (1986), An air-sea interaction theory for tropical cyclones. Part I: Steady state maintenance, *J. Atmos. Sci.*, *43*, 585–604.
- Emanuel, K. A., C. DesAutels, C. Holloway, and R. Korty (2004), Environmental control of tropical cyclone intensity, *J. Atmos. Sci.*, *61*, 843–858.
- Frank, W. M., and E. A. Ritchie (1999), Effects of environmental flow upon tropical cyclone structure, *Mon. Weather Rev.*, *127*, 2044–2061.
- Frank, W. M., and E. A. Ritchie (2001), Effects of vertical wind shear on the intensity and structure of numerically simulated hurricanes, *Mon. Weather Rev.*, *129*, 2249–2269.
- Fudeyasu, H., and Y. Wang (2011), Balanced contribution to the intensification of a tropical cyclone simulated in TCM4: Outer core spin-up process, *J. Atmos. Sci.*, *68*, 430–449.
- Hong, S.-Y., M.-S. Koo, J. Jang, J.-E. Kim, H. Park, M.-S. Joh, J.-H. Kang, and T.-J. Oh (2013), An evaluation of the software system dependency of a global atmospheric model, *Mon. Weather Rev.*, *141*, 4165–4172.
- Jones, S. C. (1995), The evolution of vortices in vertical shear. Part I: Initially barotropic vortices, *Q. J. R. Meteorol. Soc.*, *121*, 821–851.
- Jones, S. C. (2004), On the ability of dry tropical-cyclone-like vortices to withstand vertical shear, *J. Atmos. Sci.*, *61*, 114–119.
- Lorenz, E. N. (1996), Predictability—A problem partly solved, in *Proceedings of Seminar on Predictability*, Eur. Cent. for Medium-Range Weather Forecast, pp. 1–18, Reading, U. K.
- Melhauser, C., and F. Zhang (2012), Practical and intrinsic predictability of severe and convective weather at the mesoscales, *J. Atmos. Sci.*, *69*, 3350–3371.
- Molinari, J., and D. Vollaro (2010), Rapid intensification of a sheared tropical storm, *Mon. Weather Rev.*, *138*, 3869–3885.
- Molinari, J., P. Dodge, D. Vollaro, K. Corbosiero, and F. Marks Jr. (2006), Mesoscale aspects of the downshear reformation of a tropical cyclone, *J. Atmos. Sci.*, *63*, 341–354.
- Moskaitis, J. R. (2010), The predictability of tropical cyclone intensity: Results from a simple dynamical model, paper presented at 29th Conference on Hurricanes and Tropical Meteorology, Amer. Meteorol. Soc., Tucson, Ariz.
- Munsell, E. B., F. Zhang, and D. P. Stern (2013), Predictability and dynamics of a non-intensifying tropical storm: Erika (2009), *J. Atmos. Sci.*, *70*, 2505–2524.
- Nguyen, V. S., R. K. Smith, and M. T. Montgomery (2008), Tropical-cyclone intensification and predictability in three dimensions, *Q. J. R. Meteorol. Soc.*, *134*, 563–582.
- Nolan, D. S. (2011), Evaluating environmental favorableness for tropical cyclone development with the method of point-downscaling, *J. Adv. Model. Earth Syst.*, *3*, M08001, doi:10.1029/2011MS000063.
- Nolan, D. S., and M. G. McGauley (2012), Tropical cyclogenesis in wind shear: Climatological relationships and physical processes, in *Cyclones: Formation, Triggers, and Control*, edited by K. Oouchi and H. Fudeyasu, chapter 4587, pp. 1–34, Nova Sci. Publ., Happaugue, N. Y.
- Rappin, E. D., and D. S. Nolan (2012), The effect of vertical shear orientation on tropical cyclogenesis, *Q. J. R. Meteorol. Soc.*, *138*, 1035–1054.
- Reasor, P. D., and M. T. Montgomery (2001), Three-dimensional alignment and corotation of weak, TC-like vortices via linear Vortex Rossby Waves, *J. Atmos. Sci.*, *58*, 2306–2330.
- Reasor, P. D., M. T. Montgomery, and L. D. Grasso (2004), A new look at the problem of tropical cyclones in vertical shear flow: Vortex resiliency, *J. Atmos. Sci.*, *61*, 3–22.
- Rogers, R., S. S. Chen, J. Tenerelli, and H. Willoughby (2003), A numerical study of the impact of vertical shear on the distribution of rainfall in hurricane bonnie (1998), *Mon. Weather Rev.*, *131*, 1577–1599.
- Rotunno, R., and K. A. Emanuel (1987), An air-sea interaction theory for tropical cyclones. Part II: Evolutionary study using a nonhydrostatic axisymmetric numerical model, *J. Atmos. Sci.*, *44*, 542–561.
- Sippel, J. A., and F. Zhang (2008), A probabilistic analysis of the dynamics and predictability of tropical cyclogenesis, *J. Atmos. Sci.*, *65*, 3440–3459.
- Sippel, J. A., and F. Zhang (2010), Factors affecting the predictability of hurricane Humberto (2007), *J. Atmos. Sci.*, *67*, 1759–1778.
- Tang, B., and K. Emanuel (2012), A ventilation index for tropical cyclones, *Bull. Amer. Meteorol. Soc.*, *93*, 1901–1912.
- Tao, D., and F. Zhang (2014), Effect of environmental shear, sea-surface temperature and ambient moisture on the formation and predictability of tropical cyclones: An ensemble-mean perspective, *J. Adv. Model. Earth Syst.*, *6*, 384–404, doi:10.1002/2014MS000314.
- Taraphdar, S., P. Mukhopadhyay, R. L. Lueng, F. Zhang, S. Abhilash, and B. N. Goswami (2014), The role of moist processes in the intrinsic predictability of Indian Ocean cyclones, *J. Geophys. Res. Atmos.*, *119*, 8032–8048, doi:10.1002/2013JD021265.
- Torn, R., and D. Cook (2013), The role of vortex and environment errors in genesis forecasts of hurricanes Danielle and Karl (2010), *Mon. Weather Rev.*, *141*, 232–251.
- Wang, Y. (2009), How do outer spiral rainbands affect tropical cyclone structure and intensity?, *J. Atmos. Sci.*, *66*, 1250–1273.
- Wong, L. M., and C. L. Chan (2004), Tropical cyclone intensity in vertical wind shear, *J. Atmos. Sci.*, *61*, 1859–1876.
- Zhang, F., and J. A. Sippel (2009), Effects of moist convection on hurricane predictability, *J. Atmos. Sci.*, *66*, 1944–1961.
- Zhang, F., and D. Tao (2013), Effects of vertical wind shear on the predictability of tropical cyclones, *J. Atmos. Sci.*, *70*, 975–983.
- Zhang, F., C. Snyder, and R. Rotunno (2002), Mesoscale predictability of the “surprise” snowstorm of 24–25 January 2000, *Mon. Weather Rev.*, *130*, 1617–1632.
- Zhang, F., C. Snyder, and R. Rotunno (2003), Effects of moist convection on mesoscale predictability, *J. Atmos. Sci.*, *60*, 1173–1185.
- Zhang, F., N. Bei, R. Rotunno, C. Snyder, and C. C. Epifanio (2007), Mesoscale predictability of moist baroclinic waves: Convection-permitting experiments and multistage error growth dynamics, *J. Atmos. Sci.*, *64*, 3579–3594.